Optical Sectioning Microscopy at 'Temporal Super-Resolution'

Katja Flügel, Qinghai Tian, and Lars Kaestner

General Introduction

Within the recent years several super-resolution microscopic methods were developed, where the super-resolution refers to bringing the optical resolution beyond the diffraction limit introduced by Ernst Abbe, which was believed to be a real limit for quite some time. The popularity of the method also in cardiac related research can be followed in the chapter 'Quantitative super-resolution microscopy of cardiac myocytes' in this book. In parallel to this spatial super-resolution progress, within the past two decades there was a dynamic development of high speed–high resolution imaging initially towards video-rate (30 frames per second, also referred to as 'real time'-imaging) but soon to ever increasing frame rates reaching the kHz order of magnitude these days. Many processes, especially those in excitable cells such as neurons and cardiomyocytes [1] or cells in flow like erythrocytes or leukocytes [2], require even higher temporal resolution to elucidate the kinetics of processes like the Excitation-Contraction Coupling (ECC). Such ultra high speed recordings still require a diffraction limited spatial resolution to correlate function and subcellular structures [3]. Within this chapter we review optical sectioning microscopy and their application in cellular cardiology. In this approach we focus on methods that allow to access any part of the cell, i.e. we exclude methods that are intrinsically limited to surface investigations like total internal reflection fluorescence (TIRF) microscopy [4] or scanning near field optical microscopy (SNOM) [5]. In similarity we exclude techniques that require several images to

K. Flügel · Q. Tian
Theoretical Medicine and Biosciences, Saarland University, Homburg/Saar, Germany

L. Kaestner (✉)
Theoretical Medicine and Biosciences, Saarland University, Homburg/Saar, Germany

Experimental Physics, Saarland University, Saarbrücken, Germany

calculate an image section such as deconvolution microscopy [6] or structured illumination microscopy [7] (e.g., Apotome.2, Zeiss, Jena, Germany).

Confocal Microscopy

The basic principle of laser scanning confocal microscopy is an optical sectioning of the specimen along the optical axis. This is achieved by excitation of a diffraction limited spot and excluding light originating from above or below the plane of focus by fixed pinholes or variable irises depending on the construction of the confocal microscope. The price one has to pay for the optical sectioning capabilities offered with this approach is that measurements can only be obtained at a single point. Hence confocal imaging is a scanning process that can be realised by numerous scanning concepts as outlined below.

Single Beam Options

In the very initial design of a confocal microscope, Marvin Minsky used to scan the sample, i.e. the microscope stage across a stationary light beam [8]. Although this is still commercially available, especially for single molecule applications (e.g., MicroTime 200, PicoQuant, Berlin, Germany), this scanning process is inherently too slow to be further considered in this chapter. The faster alternative is scanning a single laser beam across the specimen. This method is the widely used and popular standard approach. Single beam scanners are usually equipped with galvanometer-based scanning mirrors for both, the x- and the y-direction. While this keeps the scanning electronics and the acquisition algorithms reasonably simple, this method is still relatively slow because the mirrors have to be moved physically. While conventional scanners are usually limited to single-figure frames per second, latest developments like digital controlled scan mirrors in combination with water-cooled galvanometers (e.g., LSM 880, Zeiss, Jena, Germany) can reach similar frame rates as resonating mirrors (see below).

Another well-proved concept to an increased frame rate is to switch from conventional mirrors to resonating mirrors (at least in the more demanding x-direction). When doing this, frame rates can easily reach video or double video rate (e.g., TCS SP8, Leica, Mannheim, Germany or A1R+, Nikon, Tokyo, Japan). One of the major difficulties with such an approach is the fact that the scanning process is not linear, thus sinusoidal scanning has to be accounted for with rather complex optical and/or electronics designs for compensation. In practice this leads to a selection of the most 'linear part' of the sinusoidal scan resulting in a loss of more than two thirds of the scanning time. The combination of this loss with the high frame rate results in very short pixel dwell times (as low as 25 ns).

Yet another approach to further gain one order of magnitude of scanning speed is to substitute the x-scanning mirror by an **a**custo **o**ptical **d**eflector (AOD) crystal (e.g., VT-Eye, VisiTech, Sunderland, UK). This mass-free scanning pushes the frame rate up to several hundred Hertz. The price for this speed is a reduced spatial resolution.

Caused by the design of AOD-scanning, both x- and z-direction have a slightly decreased optical resolution. This is because the AOD operates wavelength dependent and can therefore, due to the Stokes shift of the fluorescent dyes, not be used for the de-scanning as it is usually implemented in confocal heads based on scanning mirrors. This lack of descanning results in a linear moving point of the emitted fluorescence instead of a stationary point as in conventional scanners. This linearly moving point at the level of the detector excludes the implementation of a pinhole but its' replacement by a slit. For this kind of devices the restriction in scanning speed in experiments is no longer the scanning mechanism itself but most often the amount of fluorescence light available and the viability of the cells like the cardiomyocytes.

Multi Beam Options

A totally different approach of increasing the frame-rate of confocal scanning is the idea of exciting with more than one beam simultaneously. This can be realised either by a linear array of points (a line) such as the swept field microscope (e.g., Opterra II, Bruker, Billerica, MA, USA) or by a two-dimensional array of points. Since the incarnations of the latter ones use several thousands of parallel scanning beams they are referred to as kilobeam-scanners. They have many advantageous properties that are essential for imaging the dynamic behaviour of cells like cardiomyocytes. These advantages comprise beside the high acquisition speed (as fast as the attached camera can capture images), high efficiency in terms of simultaneous imaging of thousands of beams, low bleaching and low photo toxicity [9]. These kilobeam-scanners are available in two versions: The historical first version is the Nipkow-disc system, which is based on a rotating disc with a specific pattern of pinholes originally invented, designed and built to code and transmit TV images [10]. This scanning principle was made popular some 20 years ago, when the first confocal scanning units became commercially available (CSU-10, Yokogawa, Tokyo, Japan). One of the major drawbacks of spinning disc systems when reaching ultra high speed imaging, is the synchronisation of the sectors of the rotating disc with the acquisition of the camera. A system where such a synchronisation is intrinsically implemented is the so-called 2D-array scanner (e.g., VT-Infinity IV, VisiTech, Sunderland, UK). In such a device the array of parallel laser beams generated by a microlens array is actively moved across the specimen. Here, in contrast to the Nipkow disc system, the microlens- and pinhole-arrays are stationary. The only moving part is a single mirror responsible for scanning and de-scanning on the front surface as well as rescanning the image across the detection camera on its back surface. A schematic drawing of the 2D-array scanner is provided in Fig. 1. This approach ensures absolute synchrony between the scanning and the detection side of the confocal head. This concept of the 2D-array scanner also includes changeable pinhole sizes for variable resolutions in the direction of the optical axis, a feature not found in current versions of Nipkow disc based systems. Furthermore, this 2D-array scanner is now also available in a spatial super-resolution version (resolution improvement by factor of 2) based on structured illumination (VT-iSIM, Visitech, Sunderland, UK) without compromising in the recording speed.
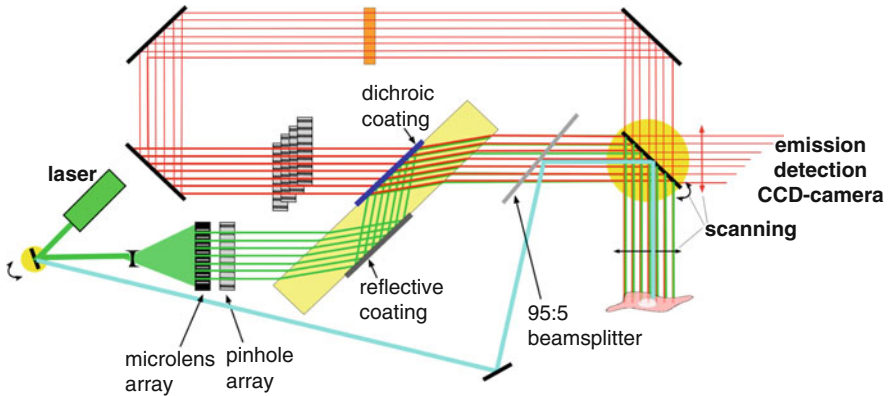
Fig. 1 A schematic design of the kilo-beam array scanner. A laser beam is widened, and a complementary stationary system consisting of a micro-lens array and a pinhole array generates a set of 50×50 beams. These beams pass through a dichroic mirror design that is insensitive to slight position changes and can be quickly changed by a motorised filter wheel. The beam bundle hits the major scanning mirror and serves three functions, scanning, de-scanning and, on its backside, re-scanning. Between the latter two functions, the emitted light passes the dichroic mirror and stationary pinhole array that consists of a set of five different pinhole sizes as well as an emission filter (orange). An additional beam path (cyan) illustrates the possibility of performing manipulations in a region of interest within the image, such as fluorescence redistribution after photobleaching (FRAP). This Figure is a reprint from Kaestner 2013 [3]

One of the most frequently used preconceptions about kilobeam scanners is the possible crosstalk between the pinholes, most prominent in thicker specimens. This will result in a diminished sectioning ability when recording 3D stacks for reconstructions [11]. However, recently kilobeam scanners with an increased distance between the pinholes became commercially available (e.g., CSU-W1, Yokogawa, Tokyo, Japan).

Beside the "true" confocal point and multi point scanner there is a variant available that inherently bears high-speed recordings: Slit-scanners do not use an individual point, but an entire line for excitation. Consequently the pinhole is replaced by a slit. The idea is to gain acquisition speed (matching the AOD-driven scanner) by sacrificing some of the resolution. This technique is currently not commercially available.

Analysis Algorithms

As outlined above, researchers are technically able to follow fast subcellular signalling in living cells, such as ECC in cardiac myocytes [12]. Decreasing the single pixel dwell times and concomitant decreases in the signal-to-noise ratio have limited the progress. However, scientific interest is not limited to the occurrence of Ca^{2+}-signals per se but also focuses on where, how much and how fast the Ca^{2+} increases occur because the signalling information is encoded in all of these properties

Fig. 2 Pixel Wise Fitting of fast 2D confocal data over time. (**a**) Raw images of 2D confocal data during the upstroke phase of an electrically evoked Ca^{2+} transient in a single rat ventricular myocyte loaded with fluo-4. Scale bar: 10 μm. (**b**) Upper panel: plot of the single-pixel fluorescence over time (blue dots) and the single-pixel PWF data (red line). Lower panel: plot of the residual over time for the single-pixel data. (**c**) The same plots as in (**b**) but for globally averaged fluorescence data. (**d**) Surface representation of the pseudo-linescan data along the yellow dashed line of the cell image for raw data (left panel) and after PWF (right panel). The arrows mark the time point of the electrical stimulation. This figure is reproduced from [26], with permission from Wolters Kluwer
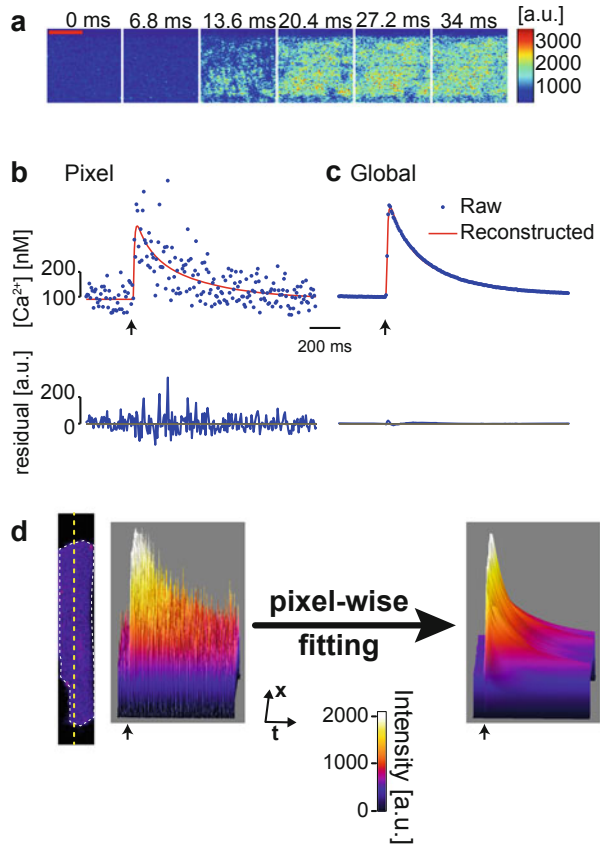
[13]. Although the analysis of the 'where' can still be achieved using data with low signal-to-noise ratios, quantitative analysis, such as determining 'how much' and 'how fast', requires data with high signal-to-noise levels. Image quality could be improved by sacrificing a spatial dimension [14], but so-called linescan imaging does not appear to adequately capture all of the necessary spatial aspects of cardiac ECC because a single line only represents approximately 1.5% of the entire confocal cross section. Figure 2a depicts typical raw images from confocal recordings of a cardiomyocyte during the onset of an electrically evoked Ca^{2+} transient that was acquired at a frame rate of 146 Hz. It appears obvious from the individual images (Fig. 2a) and from the plot of the single-pixel fluorescence over time (Fig. 2b, blue dots) that single-pixel data are extremely noisy (signal coefficient of variation: 43% at baseline Ca^{2+}). Within such data, several sources of noise limit the detailed analysis of the spatiotemporal aspects of Ca^{2+} signalling and render interpretation difficult. To overcome such restrictions analysis algorithms were developed, such as the pixel wise fitting as outlined for Ca^{2+} transients in Fig. 2c. Thus, the entire Ca^{2+} transient image stack was reconstructed and compared with the raw data (Fig. 2d).

Examples from Cardiac Ca^{2+}-Handling

The pixel-wise fitting provides, for example, new mechanistic insights in a phenomenon called Ca^{2+} transient alternans, which is the cellular equivalent of T-wave alternans in the ECG that is associated with a plethora of disease situations [15, 16]. Figure 3 shows the comparison of manifested Ca^{2+} alternans (right column) with the period preceding these macroscopic alternans (left column) in rat myocytes. For Fig. 3a–c, left column, no obvious changes occurred relative to the 'healthy' situation. In the macroscopic alternans condition, a restricted response is evident in only part of the myocytes. Despite this difference, one can find coupling sites (Fig. 3a, yellow arrows) that displayed alternating amplitudes of microscopic Ca^{2+} transients (Fig. 3d). The red traces represent the local Ca^{2+} transients as a result of
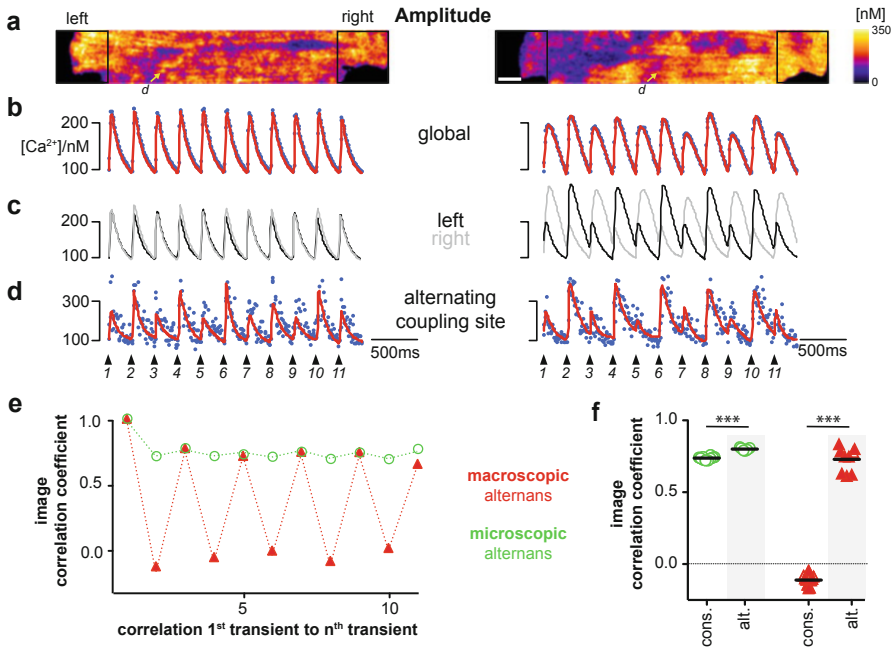
Fig. 3 Pixel Wise Fitting analysis revealed microscopic and macroscopic alternans in cardiac myocytes. Rat ventricular myocytes were loaded with fluo-4 and subjected to a step-wise increase in the stimulation frequency from 1 to 4 Hz [27]. The left column depicts the results of the analysis shortly after the increase in frequency, and the right column shows the results associated with the severe global, macroscopic alternans at a later time point. (**a**) The amplitude of the PWF. Scale bar: 10 μm. (**b**) The raw (blue dots) and reconstructed global Ca^{2+} transients (red trace). (**c**) The average of signals from the regions marked with black boxes in (**a**). (**d**) The single-pixel data (arrows in (**a**); raw: blue dots; reconstructed: red line). (**e, f**) Image correlation analysis for the distribution of the amplitude for microscopic (green) and macroscopic (red) alternans. For a detailed description, please see the text. These results were representative of seven ventricular myocytes that were studied under identical conditions. This figure is reproduced from [26], with permission from Wolters Kluwer. A more detailed comparison between the microscopic and macroscopic alternans is provided in a supplementary video 2 in the original publication [26]

PWF. The behaviour of those Ca^{2+} transients preceding the macroscopic alternans was called microscopic alternans. Quantification of the alternating behaviour was achieved by calculating the correlation coefficient between the amplitude distribution images (as depicted in Fig. 3a) of the first and all successive transients (Fig. 3e). Although the correlation was slightly but significantly changed between the consecutive and alternating transients during microscopic alternans (marked in green circles; Fig. 3f), the macroscopic alternans resulted in an alternation between large positive and negative values for the image correlation coefficient (marked in red triangels, Fig. 3e, f). These data revealed quantitative information about the subtle details of ECC in cardiac myocytes during the onset of alternans.

Going further into details, it would be desirable to monitor the activity of individual ECC sites (couplons), especially since plasmalemma and sarcoplasmic reticulum membrane calcium channels are important determinants of the heart's performance. The astronomer's CLEAN algorithm [17] initially designed to observe individual stars in a galaxy was recently applied to fast confocal images of cardiac myocytes and named CaCLEAN [1]. This algorithm was shown to untangle the fundamental characteristics of ECC couplons by combining the known properties of calcium diffusion. CaCLEAN empowers the investigation of fundamental properties of ECC couplons in beating cardiomyocytes without pharmacological interventions. Upon examining individual ECC couplons at the nanoscopic level, their roles in the negative amplitude-frequency relationship and in β-adrenergic stimulation, including decreasing and increasing firing reliability, respectively, was reviled as depicted in Fig. 4A, B. CaCLEAN combined with 3D confocal imaging of beating cardiomyocytes provides a functional 3D map of active ECC couplons (on average, 17,000 per myocyte) as shown in Fig. 4C. In future, CaCLEAN will enlighten the ECC-couplon-remodelling processes that underlie cardiac diseases.

Non-linear Microscopy

The idea behind non-linear microscopy (NLM) is to condense the laser energy in time (femto-second pulses) and space (focus) such that the energy density in the focus becomes so high that the photons and the molecule of the sample interact in a non-linear manner. This NLM can either be based on fluorescence (multi photon microscopy) or on the interaction with so called non-linear materials leading to a frequency multiplication like second harmonic generation (SHG) or third harmonic generation (THG).

Multi Photon Microscopy

In multi photon microscopy, the dye absorbs two (or multiple) photons simultaneously. Since the underlying molecular excitation process remains the same, both photons have to deliver approximately half (or other fractions depending on the multiplicity of excitation) of the energy. Half of the energy translates into a doubling of the wavelength, which explains why far red and infrared light emitting Titan:Sapphire lasers are
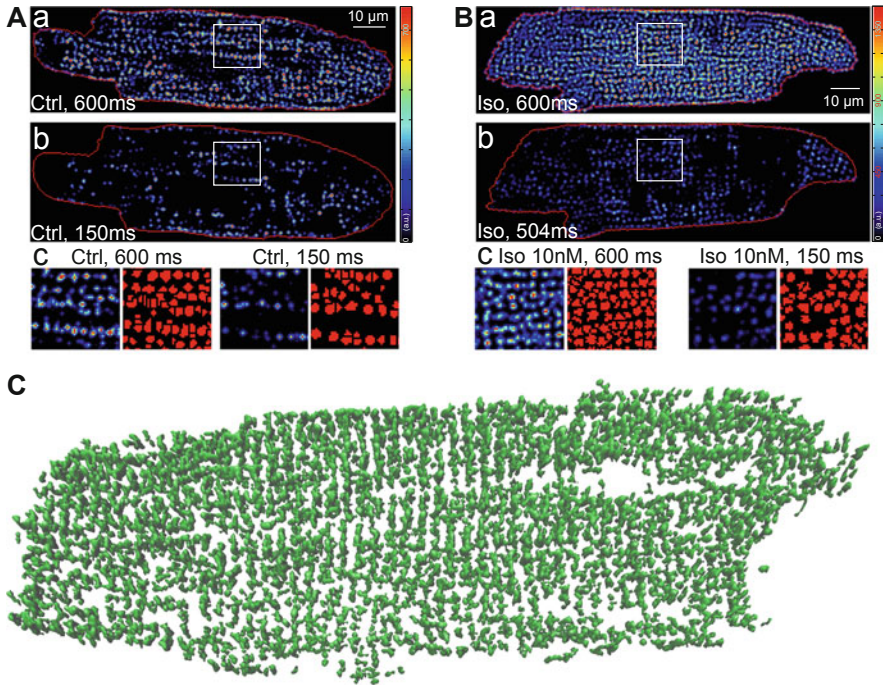
Fig. 4 Behavior of ECC couplons at variable stimulation frequencies and during β-adrenergic stimulation. Rat ventricular myocytes were electrically paced into steady state at the stimulation intervals given in the images. (**A**) The resulting CaCLEAN ECC couplon maps at 600 ms (**a**) and 150 ms (**b**) stimulation intervals under control conditions (Ctrl). Subcellular regions highlighted with white boxes were replotted at a high magnification (**c**) alongside with segmented ECC couplon sites (**c**, red). (**B**) Data similar to those in (**A**) but in a ventricular myocyte following β-adrenergic stimulation (10 nM isoproterenol, 5 min) (Iso). (**C**) Three-dimensional reconstruction of active ECC couplons in a naïve rat ventricular myocyte. Panels (**A**) and (**B**) are reproduced from [1], with permission from eLife Sciences Publications, Ltd

popular. Thus, if the chromophore requires, e.g., single photon excitation at 450 nm, the equivalent two-photon excitation wavelength would be 900 nm. For other multi photon processes this shift is multiplied by higher factors. One should be aware that the absorption cross-section of single photon and multi photon excitation can be quite different. The basic advantage of multi photon microscopy compared to single photon confocal imaging is reduced photobleaching in out-of-focus planes, since the multi photon excitation is restricted to the focal plane. For a thorough discussion of multi photon microscopy see [18]. Here, we solely mention two additional significant advantages of multi photon excitation. (a) Deeper penetration depth. Since excitation can be performed with red, far-red or even infrared light the penetration of the excitation light in living tissue is considerably increased in comparison to shorter wavelengths. Hence it is possible to image single cardiac myocytes in the intact heart as outlined in
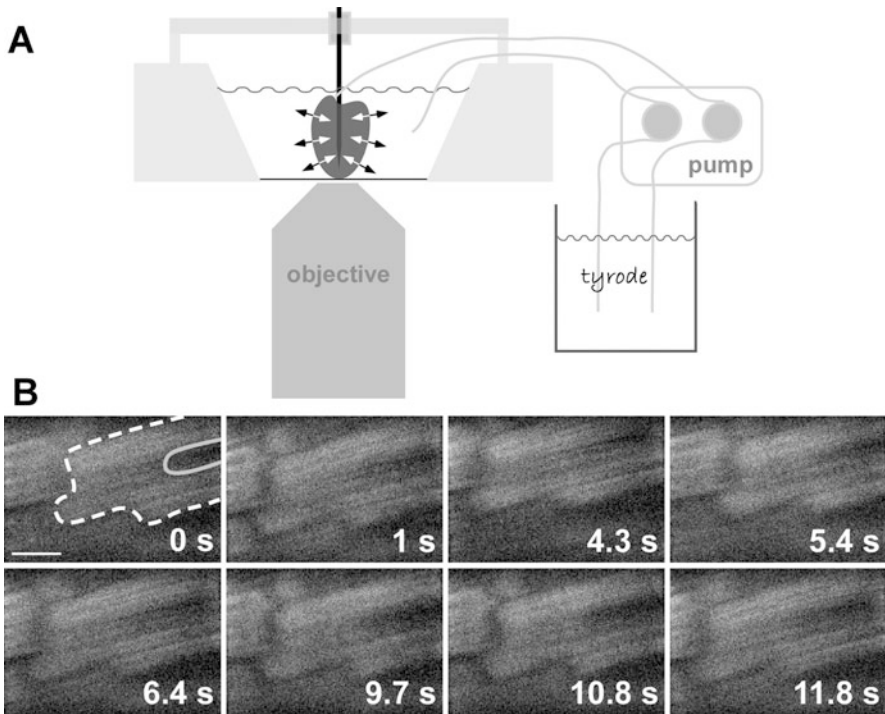
Fig. 5 Imaging of a perfused beating mouse heart. Panel (**A**) shows the design of the measuring chamber for use with an inverted microscope. In order to minimise motion artefacts the heart was fixed by a needle (black vertical line in panel A), the needle was placed exactly in the optical axis of the microscope objective. Since the heart was 'beating around' the needle (illustrated by the arrows) a virtually motion-free image could be recorded. A peristaltic pump was employed for continuous retrograde perfusion. Panel (**B**) depicts representative autofluorescence images of an identified myocyte throughout a recording period of 12 s (at video-rate). The scale bar represents 10 μm. The shape of the cell and the nucleus is highlighted in the first image by the dashed white line and the solid grey line, respectively. This Figure is reproduced from Kaestner and Lipp 2007 [28]

Fig. 5. It should be mentioned here that the maximal penetration depth is tissue dependent. One still has to consider that emission light scattering becomes more prominent with increasing penetration depth. (b) Intrinsic sectioning. As described above, the 'multi photon effect' is restricted to the core of the excitation light focus in the specimen due to the non-linear excitation probability. From this it follows that in contrast to single photon confocal scanners that employ optical sectioning on the 'emission' side (spatial filter, the pinhole(s)), scanners using multi photon excitation already generate sectioning on the excitation side. For single point scanners this translates into their liberation from de-scanning; all light emitted, originates exclusively from the excitation volume that is diffraction limited and thus light collection does not require the ability for spatial discrimination. Similar to single beam scanners, in multi photon microscopy the construction of a 2D image is also realised by a scanning

process. In the easiest of all cases scanning is performed by means of two galvanometer controlled mirrors with all the limitations discussed above. The application of fast AOD crystals for x-scanning is certainly more complex when using pulsed femtosecond light sources, because diffraction of AODs is wavelength dependent and fs-pulsed lasers produce a spectral band (e.g., with 75 fs pulses the bandwidth of the resulting spectrum can reach around 10 nm). This means that the degree of diffraction of the excitation light will be different for the 'red' and the 'blue' components of the excitation spectrum. Nevertheless, multiple approaches exist that offer possible solutions [19, 20]. In addition to that a multi photon multi point multi plexed scanner with up to 128 parallel excitation points arranged in a line is commercially available (TriM Scope II, LaVision BioTec, Bielefeld, Germany), where acquisition speed is practically limited by the frame rate of the camera attached.

SHG Imaging

SHG imaging can be performed in reflective and in transmission mode. This depends on the properties of the particular 'interaction material' as well as on the sample preparation. In most cases SHG imaging relies on intrinsic structures and hence no additional staining of cells or tissue is required. For example collagens give a strong reflective SHG signal. Since collagens are built up in the process of fibrosis and are also part of the vessels such parameters can be investigated in tissue sections, e.g., for human cardiac appendages as outlined in Fig. 6.

Another structure in cardiac myocytes providing a strong SHG-(transmission) signal is myosin [21], which can be used to measure sarcomere length [22] and hence to follow cellular contraction. This approach is especially interesting for stem cell derived cardiomyocytes, where the contractile structures are not as well organised as in adult cardiomyocytes and hence the classical cell length measurements [23] fail. Such SHG-imaging of contracting stem-cell derived cardiomyoctes can very well be used for functional phenotyping.
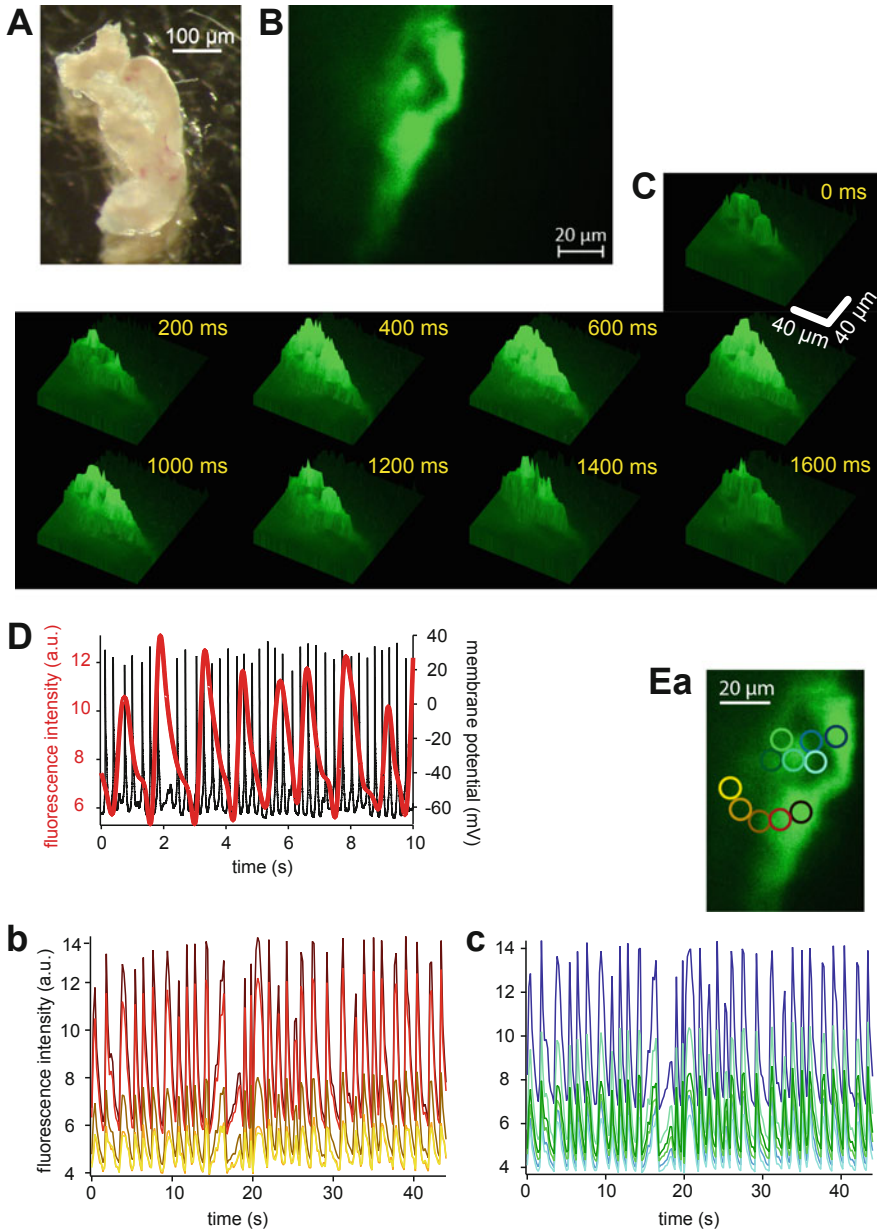
Light-Sheet Imaging

Light sheet imaging also known as selective plane imaging (SPIM) relies on the illumination of the sample by a light sheet perpendicular to the optical axis of the microscope. The recent revival of that technique [24] is based on a sample holder with a rotational axis parallel to the gravitation field that enables rotation while keeping the sample itself distortion-free. The implementation of this design became commercially available (Lightsheet Z.1, Zeiss, Jena, Germany). The serial optical sectioning is realised by moving the sample through the light sheet and for every position an image is collected. Although the lateral resolution is lower than with confocal techniques the biggest advantage of light sheet imaging is its ability to reach the same optical resolution in all three spatial dimensions. Similar but not identical to multi photon excitation light sheet excitation happens exclusively in
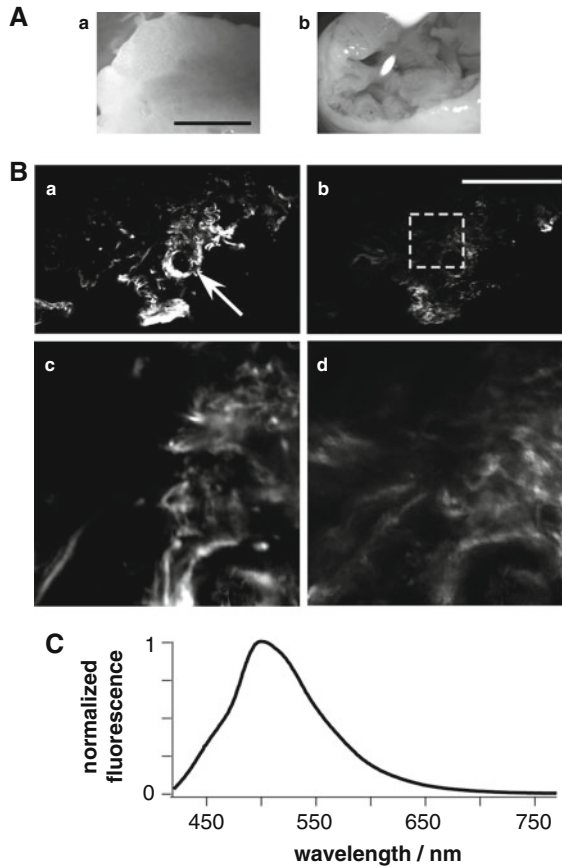
Fig. 6 Non-linear imaging of human auricles. Panel (**A**) shows the macroscopic appearance of the atrial appendages; (**Aa**)—from outside the heart (epicardial side) and (**Ab**) from inside the heart, where the surgical cut was performed. The scale bar represents 5 mm. Panel (**B**) depicts laser scanning images taken from inside an atrial appendage as shown in image (**Ab**). Images (**Ba**) and (**Bc**) display the SHG reflection signal indicating elastin and collagen fibres of the extracellular matrix, while images (**Bb**) and (**Bd**) represent the same image section viewed at the autofluorescence wavelengths. The spherical structure in (**Ba**) marked by the white arrow resembles a small vessel. The dashed square in image (**Bb**) shows the section that was scanned at a higher magnification for panels (**Bc**) and (**Bd**). The scale bar represents 50 μm for panels (**Ba**) and (**Bb**), and 10 μm for panels (**Bc**) and (**Bd**). Panel (**C**) provides a fluorescence spectrum of the autofluorescence from panels (**Bb**) and (**Bd**) upon excitation with 410 nm light. This Figure is reproduced from Kaestner and Lipp 2007 [28]

the focal plane, avoiding bleaching outside the focus. When imaging 3D-stacks, acquisition speed is limited, however, when imaging, e.g., dynamic processes, in a single plane, speed is only determined by the operation of the camera. Heavy computational power has to be invested before a 3D-reconstruction can be visualised, but also for this task reliable solutions are commercially available, e.g.,

Fig. 7 Light sheet imaging of Ca^{2+}-signals in a sinoatrial node (SAN). (**A**) depicts a white light image of a SAN isolated from a mouse with tissue-specific expression (HCN4 KiT Cre) of the genetically encoded Ca^{2+} sensor GCaMP3. (**B**) shows a representative Light sheet recording of the SAN specific expression of GCaMP3 using a Zeiss Z.1 microscope. (**C**) presents a time series of surface plots of Ca^{2+}-signals of the autonomously beating SAN depicted in panels (**A**) and (**B**). The fluorescence activity of particular (pacemaker) cells can be identified. (**D**) compares the time course of the Ca^{2+}-signals of the SAN with action potentials measured by patch-clamp in isolated

Vision4D (arivis, Rostock, Germany). Although manipulation of the sample (e.g., by patch-clamp) is more complicated or impossible, the placement of the sample in 3D is easier and has more degrees of freedom than placing a sample on a coverslip like in conventional microscopy. An example where such an option is advantageous is given in Fig. 7, where a sinoatrial node (SAN) expressing a genetically encoded Ca^{2+} indicator (GCaMP3, compare chapter 'Optogenetic Tools in the Microscopy of Cardiac Excitation-Contraction Coupling'), was isolated from a mouse heart. In the current implementation of light-sheet imaging, excitation manipulation still needs to be synchronised with the camera, which is a major limitation of the acquisition speed that has the potential to increase in future.

Conclusions

Speaking about (diffraction limited) imaging speed, temporal resolution can always be increased by sacrificing spatial resolution. The first step in this concept would be the reduction of the number of pixels per image. This can be realised either by limiting the overall size of the image or by binning adjacent pixels or at its extreme by reducing image sizes to individual lines (line-scans). Going further—if the entire fluorescence signal of the microscope is detected in a point detector we speak about confocal spot measurements [25]. In this case sampling rates can be as high as several MHz. Nonetheless, even without any special optical spatial resolution, e.g., video imaging, the functional spatial resolution can originate from the experimental design (see FRET in the chapter 'Optogenetic Tools in the Microscopy of Cardiac Excitation-Contraction Coupling') and does not only exceed the diffraction limit but optical super-resolution.

As we described in this chapter, particular experimental designs in cellular cardiology exploring the cellular and molecular regulation of ECC, may require special high speed sectioning microscopy methods. All of them bear advantages and disadvantages and therefore need to be carefully selected, proscribing a general recommendation in favour of a particular technology and it's implementation.

Fig. 7 (continued) SAN-cells showing a higher frequency relative to the intact SAN. (**E**) provides a spatio-temporal analysis of Ca^{2+}-signals in the autonomously beating SAN. (**a**) shows the regions of interest (ROIs) analysed. ROIs are arranged in two groups with traces depicted in (**b**) and (**c**). The colour code of the ROIs in (**a**) corresponds with the colour traces in (**b**) and (**c**). The acquisition rate is too low to identify particular spots of Ca^{2+}-signal origin or a spatio-temporal spreading of the signals. However, there is a clear indication of an interconnection of the different ROIs, even between the two grouped ones, because any kind of arrhythmic episodes or major intensity changes are evident in all ROIs

References

1. Tian Q, Kaestner L, Schröder L, Guo J, Lipp P. An adaptation of astronomical image processing enables characterization and functional 3D mapping of individual sites of excitation-contraction coupling in rat cardiac muscle. Elife. 2017;6:665.
2. Quint S, et al. 3D tomography of cells in micro-channels. Appl Phys Lett. 2017;111:103701.
3. Kaestner L. Calcium signalling. Approaches and findings in the heart and blood. New York, NY: Springer; 2013.
4. Poulter NS, Pitkeathly WTE, Smith PJ, Rappoport JZ. The physical basis of total internal reflection fluorescence (TIRF) microscopy and its cellular applications. Methods Mol Biol. 2015;1251:1–23.
5. Micheletto R, et al. Observation of the dynamics of live cardiomyocytes through a free-running scanning near-field optical microscopy setup. Appl Optics. 1999;38:6648–52.
6. Carrington W, Fogarty K. 3-D molecular distribution in living cells by deconvolution of optical sections using light microscopy. In: Foster KR, editor. Proceedings of 13th Annual Northeast Bioengineering Conference. New York, NY: IEEE Press; 1987. p. 108–11.
7. Neil MA, Juskaitis R, Wilson T. Method of obtaining optical sectioning by using structured light in a conventional microscope. Opt Lett. 1997;22:1905–7.
8. Minsky M. Microscopy apparatus. 1957.
9. Lipp P, Kaestner L. In: Hüser J, editor. High throughput-screening in drug discovery. Weinheim: Wiley-VCH; 2006. p. 129–49.
10. Nipkow P. Elektrisches teleskop. 1884.
11. Egner A, Andresen V, Hell SW. Comparison of the axial resolution of practical Nipkow-disk confocal fluorescence microscopy with that of multifocal multiphoton microscopy: theory and experiment. J Microsc. 2002;206:24–32.
12. Bers DM. Cardiac excitation-contraction coupling. Nature. 2002;415:198–205.
13. Berridge MJ, Bootman MD, Lipp P. Calcium--a life and death signal. Nature. 1998;395:645–8.
14. Tian Q, et al. Functional and morphological preservation of adult ventricular myocytes in culture by sub-micromolar cytochalasin D supplement. J Mol Cell Cardiol. 2012;52:113–24.
15. Weiss JN, Nivala M, Garfinkel A, Qu Z. Alternans and arrhythmias: from cell to heart. Circ Res. 2011;108:98–112.
16. Laurita KR, Rosenbaum DS. Cellular mechanisms of arrhythmogenic cardiac alternans. Prog Biophys Mol Biol. 2008;97:332–47.
17. Högbom JA. Aperture synthesis with a non-regular distribution of interferometer baselines. Astron Astrophys Suppl. 1974;15:417–26.
18. Denk W, Piston DW, Webb WW. In: Pawley JB, editor. Handbook of biological confocal microscopy. New York, NY: Plenum Press; 1995. p. 445–58.
19. Bouzid A, Lechleiter J. Laser scanning fluorescence microscopy with compensation for spatial dispersion of fast laser pulses. Opt Lett. 2006;31:1091.
20. Roorda RD, Miesenbock G. Beam-steering of multi-chromatic light using acousto-optical deflectors and dispersion-compensatory optics. 2002.
21. Plotnikov SV, Millard AC, Campagnola PJ, Mohler WA. Characterization of the myosin-based source for second-harmonic generation from muscle sarcomeres. Biophys J. 2006;90:693–703.
22. Boulesteix T, Beaurepaire E, Sauviat M-P, Schanne-Klein M-C. Second-harmonic microscopy of unstained living cardiac myocytes: measurements of sarcomere length with 20-nm accuracy. Opt Lett. 2004;29:2031–3.
23. Viero C, Kraushaar U, Ruppenthal S, Kaestner L, Lipp P. A primary culture system for sustained expression of a calcium sensor in preserved adult rat ventricular myocytes. Cell Calcium. 2008;43:59–71.
24. Huisken J, Swoger J, del Bene F, Wittbrodt J, Stelzer EH. Optical sectioning deep inside live embryos by selective plane illumination microscopy. Science. 2004;305:1007–9.
25. Parker I, Ivorra I. Confocal microfluorimetry of Ca^{2+} signals evoked in Xenopus oocytes by photoreleased inositol trisphosphate. J Physiol. 1993;461:133–65.

26. Tian Q, Kaestner L, Lipp P. Noise-free visualization of microscopic calcium signaling by pixel-wise fitting. Circ Res. 2012;111:17–27.
27. Aistrup GL, et al. Pacing-induced heterogeneities in intracellular Ca^{2+} signaling, cardiac alternans, and ventricular arrhythmias in intact rat heart. Circ Res. 2006;99:E65–73.
28. Kaestner L, Lipp P. Non-linear and ultra high-speed imaging for explorations of the murine and human heart. Prog Biophys Mol Biol. 2007;8:66330K-1–66330K-10.